Superconductor-like effects in an ac-driven normal Mott-insulating quantum dot array

Sanjeev Kumar and Vikram Tripathi
Department of Theoretical Physics, Tata Institute of Fundamental Research, Homi Bhabha Road, Navy Nagar, Mumbai 400005, India

(Received 14 February 2020; revised 7 October 2020; accepted 8 December 2020; published 22 December 2020)

We study the current response of an ac-driven dissipative Mott-insulator system, a normal quantum dot array, using an analytical Keldysh field-theory approach. Deep in the Mott-insulator regime, the nonequilibrium steady state (NESS) response resembles a resistively shunted Josephson array with a nonequilibrium Mott-insulating to conductor transition as the drive frequency Ω is increased. The diamagnetic component of the NESS in the conducting phase is anomalous, implying negative inductance, strikingly reminiscent of the η-pairing phase of a Josephson array with negative phase stiffness. However, in the presence of an additional dc field the signature of supercurrent—Shapiro steps—is completely absent. We interpret these properties as number-phase fluctuation effects shared with Josephson systems rather than superconductivity.

DOI: 10.1103/PhysRevB.102.235147

I. INTRODUCTION

The nonequilibrium response of strongly correlated quantum systems is a challenging problem requiring understanding of the many-body excitation spectra, wave functions, dynamical bottlenecks, and dissipative processes. Driven Mott insulators are a prototypical example, exhibiting diverse phenomena that are otherwise not present in their equilibrium or linear-response regimes, such as field/current driven insulator-metal transitions [1–5], Bloch oscillations or Wannier-Stark quantization [6–11], and current enhanced diamagnetism [12]. A number of recent studies of optically excited Mott-insulating half-filled Hubbard models have proposed a new route to superconductivity through doublon creation [13–22], possibly an exotic η-pairing state [23]. The evidence comes from superconductor-like properties, such as effective attractive Coulomb correlations [13,19,21], finite charge stiffness [24], and off-diagonal long-range order parameter correlations [15,24,25]. However these half-filled Hubbard models are special since charge excitations necessarily create doublons. We, therefore, ask whether superconductor-like properties may still be seen in driven Mott insulators where charge excitations are not associated with doublons. Specifically, we study the current response of a dissipative Mott insulator system—an array of mesoscopic quantum dots each with a large and arbitrary number of interacting electrons—to an ac electric-field quench.

We find that the NESS response deep in the Mott-insulator regime has a striking resemblance with optically driven resistively shunted Josephson arrays on either side of a superconductor-insulator transition. We show that the frequency dependence of the current response has regimes of both diamagnetic and insulating behavior as the ac drive tunes the Mott insulator through a singularity separating insulator and metallic frequency dependences of the optical conductivity, indicating a nonequilibrium insulator-metal transition. However the sign of the diamagnetic response is anomalous (negative), tantamount to π-phase slips in the links, analogous to the η-pairing phase of Josephson arrays with negative phase stiffness. In the presence of a simultaneous dc bias, the dc IV characteristics exhibit Josephson-like photon-mediated tunneling in the form of current steps at bias values separated by integer multiples of drive frequency $\hbar\Omega/e$, but crucially, Shapiro steps—a key signature of supercurrent—expected at integer multiples of $\hbar\Omega/2e$ are absent, unlike the observation in Josephson systems [26–28]. We propose that the similarities shared with the reported optical response of Mott insulators are not on account of η-pairing or ac-induced superconductivity but are a manifestation of number-phase duality effects common to both. Strong charge fluctuations, whether associated with underlying superconductivity or optical pumping, suppress quantum fluctuations of the phases.

Theoretical understanding of driven Mott insulators has received a significant impetus by developments in the Keldysh dynamical mean-field theory (KDMFT) approach [8,9,11,29–32], tensor network techniques [25], and the analytic Bethe ansatz [33] including the effective $\mathcal{PT}$-symmetric descriptions [34,35]. Recently an alternate analytical large-$\mathcal{N}$ effective Keldysh field-theory approach [6] has been developed based on the well-known Ambegaokar-Eckern-Schön (AES) rotor model [36,37] for electron transport in mesoscopic quantum dot arrays, effectively a dissipative Mott-insulator system. This Keldysh formalism captures numerous nonequilibrium dc phenomena including Bloch-like oscillations and the field-driven insulator to metal transition. It also provides an analytical treatment of the approach to the NESS. Here we will generalize this formalism for the ac response.

The rest of the paper is organized as follows. In Sec. II we introduce the Keldysh AES model for transport in a quantum dot chain and obtain an expression for the current response functional. Section III is devoted to the study of the current response to a uniform ac drive. The analysis not only confirms a number of results, such as odd harmonic generation, Bloch-like oscillations, and effective attractive

local Coulomb correlations, hitherto obtained from numerical KDMFT studies, but also reveals some aspects missed in the numerical studies, most notably the slow decay of the Bloch-like oscillations. We find striking similarities to the current response of superconductor Josephson junction arrays with effectively negative superfluid stiffness, reminiscent of an η-pairing phase. To check if the superconductor-like optical response is indeed due to superconductivity in our system, we analyze in Sec. IV the current response when ac and dc-driving fields are simultaneously present. Although photon-mediated tunneling features, similar to superconducting Josephson arrays are also found here, the absence of Shapiro steps, a key signature of supercurrent, leads us to conclude that the properties are a manifestation of number-phase duality shared with superconductors. Section V contains a summary of our findings and a discussion.

II. MODEL AND FORMALISM

Our starting point is a model Hamiltonian of a quantum dot array,

$$H = H_0 + H_C + H_{\rm tun}, \tag{1}$$

where

$$H_0 = \sum_{k\alpha} (\epsilon_{k\alpha} - \mu) c^\dagger_{k\alpha} c_{k\alpha} \tag{2}$$

describes noninteracting electrons in the dots with energies $\epsilon_{k\alpha}$ for the kth dot,

$$H_C = E_C \sum_k \left[\left(\sum_\alpha c^\dagger_{k\alpha} c_{k\alpha} \right) - N_0 \right]^2 \tag{3}$$

represents Coulomb interaction, and

$$H_{\rm tun} = \sum_{k,\alpha\beta} t^{\alpha\beta}_{k,k+1} c^\dagger_{k\alpha} c_{k+1,\beta} + \text{H.c.} \tag{4}$$

denotes interdot tunneling. Each dot contains a large number $N_0 \gg 1$ of electrons that provide a dissipative fermionic bath with an approximate continuum of levels $\{\epsilon_{k\alpha}\}$ with mean spacing $\delta \sim O(1/N_0)$. The large number of single-electron levels in each dot also serves as a large-$\mathcal{N}$ parameter that provides useful simplifications leading to our final effective action (see below). In order to treat the tunneling effects correctly with respect to the "bare" Hamiltonian which is interacting, one follows [38] the standard process of Hubbard-Stratonovich decoupling of the interaction, and eliminating the Hubbard-Stratonovich fluctuation potentials by gauge transformations of the fermion fields. Then following Refs. [6,38] (see also the Appendix) we go over to the Keldysh path-integral formalism with the action corresponding to our Hamiltonian put on the Keldysh time contour. Thereafter the fermionic degrees of freedom are integrated out, and the resulting fermionic determinant is expanded in increasing powers of the tunneling (only even powers survive). Terms in the effective action that are $O(|t|^4)$ and higher get suppressed in the large-$\mathcal{N}$ limit. The Appendix contains an outline of these steps. The physical significance of the large-$\mathcal{N}$ approximation in suppressing higher-order tunneling terms in the effective action is illustrated in Fig. 1. Note that in one

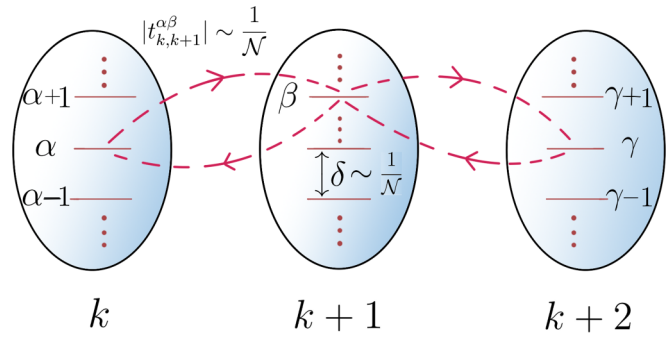

FIG. 1. Figure illustrating the tunneling processes between the normal quantum dots (labeled k, $k+1$, and $k+2$) each of which contains a large number of single-electron levels $\epsilon_{k\alpha}$. The mean level spacing $\delta \sim \mu/\mathcal{N}$, where $\mathcal{N} \gg 1$ is on the order of the number of conduction electrons in a dot, and μ is the bulk Fermi energy of the material of the dot. Transport is controlled by the dimensionless interdot tunneling conductance $g \sim |t|^2/\delta^2$, where $|t|^2$ is the mean square of the distribution of the interdot tunneling elements, assumed to be a Gaussian white-noise distribution $\langle t^{\alpha\beta}_{k,k+1} t^{\gamma\delta}_{k+1,k} \rangle = |t|^2 \delta^{\alpha\delta} \delta^{\beta\gamma}$ for simplicity and concreteness. In order for g to be physically meaningful, we require the tunneling elements $t^{\alpha\beta}_{k,k+1}$ to scale as $1/\mathcal{N}$. The figure illustrates a higher-order tunneling process involving three dots. The summation over the internal indices α, β, and γ contributes a scaling factor $\mathcal{N}^3$ whereas the four tunneling elements contribute $1/\mathcal{N}^4$. This higher-order process, thus, scales as $1/\mathcal{N}$ and may be dropped in the large-$\mathcal{N}$ limit.

or few-orbital Hubbard models, the large-$\mathcal{N}$ approximation is not available; hence, in that situation, higher-order tunneling terms must be retained in the effective rotor action.

The end result is our effective Keldysh-AES rotor action [6,38],

$$S = S_C + S_{\rm tun} \tag{5}$$

for a one-dimensional array of quantum dots each with a charging energy E_C and interdot dimensionless conductance $g \sim \langle |t^2| \rangle / \delta^2$, where

$$S_C = \frac{1}{4E_C} \sum_k \int_t [(\partial_t \phi^+_k)^2 - (\partial_t \phi^-_k)^2 + N_0 \partial_t (\phi^+_k - \phi^-_k)] \tag{6}$$

represents Coulomb correlations, and $S_{\rm tun}$, a nonlocal term, represents the interdot tunneling processes,

$$S_{\rm tun}[\phi] = g \sum_k \int_{t,t'} \begin{pmatrix} e^{-i\phi^+_{k,1}} \\ e^{-i\phi^-_{k,1}} \end{pmatrix}^T_t L_{k,1}(t,t') \begin{pmatrix} e^{i\phi^+_{k,1}} \\ e^{i\phi^-_{k,1}} \end{pmatrix}_{t'}. \tag{7}$$

Here the superscripts $\pm$ label the forward and backward parts, respectively, of the Keldysh time contour, the fields $\phi^\pm_k$ in Eq. (6) are the phases dual to the charge excitations $n^\pm_k$ (the $e^{i\phi^\pm_k}$ annihilate one charge) on the kth quantum dot. The phases $\phi^\pm_{k,1}$ in Eq. (7) are the difference fields $\phi^\pm_k - \phi^\pm_{k+1}$ across the link $(k, k+1)$. The kernel $L_{k,1}(t,t')$ is a 2×2 matrix in Keldysh ($\pm$) space with the following structure [6,38]:

$$L_{k,1} = \frac{1}{4} \begin{pmatrix} \Sigma^R_{k,1} + \Sigma^A_{k,1} + \Sigma^K_{k,1} & \Sigma^R_{k,1} - \Sigma^A_{k,1} - \Sigma^K_{k,1} \\ -\Sigma^R_{k,1} + \Sigma^A_{k,1} - \Sigma^K_{k,1} & -\Sigma^R_{k,1} - \Sigma^A_{k,1} + \Sigma^K_{k,1} \end{pmatrix}_{tt'}, \tag{8}$$

and the functions $\Sigma^{R,A,K}$ are, in turn, expressed in terms of products of the noninteracting local (in space) Green's functions $G^{R,A,K}$,

$$\Sigma^{R(A)}_{k,1}(t,t') = i\big[G^{R(A)}(t-t')G^{K}_{k}(t',t) + G^{K}_{k+1}(t,t')G^{A(R)}(t'-t)\big], \tag{9}$$

$$\Sigma^{K}_{k,1}(t,t') = i\big[G^{K}_{k}(t',t)G^{K}_{k+1}(t,t') - (G^{R}-G^{A})_{t-t'}(G^{R}-G^{A})_{t'-t}\big]. \tag{10}$$

The retarded (advanced) local Green's functions have the form $G^{R(A)} = \sum_\alpha (i\partial_t \pm i\eta - \xi_\alpha)^{-1}$ with ξ_α as the αth single-particle energy level reckoned from the dot's Fermi level (see the Appendix). The infinitesimally small positive constant η ensures the theory has proper causal structure. Likewise, $G^K_k(t,t')$ is the local Keldysh component of the noninteracting Green's function $G^K_k(t,t') = F_k(t,t')(G^R - G^A)_{t-t'}$, where F_k is related to the distribution function for the single fermion excitations in a dot. Any power dissipated in the dots will result in electron heating, which would necessitate tracking the time evolution of F_k. Therefore, for simplicity, we make the further assumption that the dot electrons are coupled to an external phonon bath and the electron relaxation time due to electron-phonon collisions is much shorter than that due to interdot electron tunneling, which is on the order of $(g\delta)^{-1}$. This allows one to replace $L_{k,1}(t,t')$ by its *equilibrium* value in which case $L_{k,1}(t,t')$ depends only on the difference of the two time arguments [6,38]. For this equilibrium case, $F_k(t,t') \equiv F_k(t-t')$, and its Fourier transform has the simple form $F_k(\epsilon) = 1 - 2f_k(\epsilon)$, where $f_k(\epsilon)$ is the equilibrium Fermi distribution function.

The tunneling action in Eq. (7) shares similarities with Josephson tunneling actions used to describe transport in superconducting dot arrays: Both involve periodic functions of the phases necessary to ensure charge quantization and feature single-particle excitation gaps. Nevertheless, there are crucial differences between the two. In Eq. (7), the kernel $L_{k,1}(t,t')$ is nonlocal in time, unlike the Josephson case where it is local in time and has a form $S_{\rm tun}[\phi] = J\sum_k \int_t \cos[2\phi(t)]$. The time nonlocality arises from integrating out the gapless particle-hole fermionic excitations in the origin and destination dots and represents the dissipative nature of the interdot tunneling process. In a Josephson junction array, the tunneling of Cooper pairs occurs without dissipation, and particle-hole excitations are subject to the superconducting gap Δ. Another difference is that the Josephson coupling $J \sim g\Delta$ explicitly depends on the superconducting gap whereas for the normal case, the tunneling term has no characteristic energy scale. However, both superconductor and normal dot chains do contain the charging term that has a characteristic scale E_C. We will see below that the similarities of the two cases result in similar optical response and serve to caution relying on certain optical properties for confirming superconductivity. However, the differences between the two cases show up in properties, such as the absence of Shapiro steps—a key signature of supercurrent—in the normal dot array.

The retarded (advanced) Green's function has a causal structure, i.e., $G^R(t) \propto \Theta(t)$ and $G^A(t) \propto \Theta(-t)$. The same causality structure is obeyed by $\Sigma^{R(A)}(t)$. Additionally, in Fourier space the following identities facilitate the calculation of expectation value of the current response,

$$\big(\Sigma^R_{k,1} - \Sigma^A_{k,1}\big)_\epsilon = \frac{i}{\pi}\epsilon, \tag{11}$$

$$\big(\Sigma^K_{k,1}\big)_\epsilon = \frac{i}{\pi}\epsilon F_b(\epsilon), \tag{12}$$

where $F_b(\epsilon) = 1 + 2f_b(\epsilon)$ with f_b as the equilibrium Bose distribution (see the Appendix). In the rest of this paper, we choose to work in units of $\hbar = e = 1$.

We introduce the external ac electric field as a time-dependent "classical" vector potential on the links $A^c_{k,1} = (A^+_{k,1} + A^-_{k,1})/2$ turned on at time $t = 0$ (a quench),

$$A^c_{k,1} = \Theta(t)(V/\Omega)\cos(\Omega t). \tag{13}$$

This changes the tunneling part of the action, Eq. (7), by incorporating Peierls shifts in the phase differences $\phi^{c,q}_{k,1}(t) \to \phi^{c,q}_{k,1}(t) + A^{c,q}_{k,1}(t)$, where $\phi^{\pm}_{k,1} = \phi^c_{k,1} \pm \phi^q_{k,1}/2$. The nonequilibrium current $\hat{j}_{k,1}[\phi]$ in a link is obtained in the usual manner by introducing infinitesimal quantum components of the vector potential $A^q_{k,1}$ and varying the action with respect to it.

Defining $e^{\pm}_{k,1}(t) = \exp[i\phi^{\pm}_{k,1}(t) - iA^{\pm}_{k,1}(t)]$, the current functional in terms of phase fields is

$$\begin{aligned}\hat{j}_{k,1}(\tau) = ig\int_t\ & [(e^+_\tau)^* L^{++}_{\tau,t} e^+_t - (e^+_t)^* L^{++}_{t,\tau} e^+_\tau \\ & + (e^+_\tau)^* L^{+-}_{\tau,t} e^-_t + (e^+_t)^* L^{+-}_{t,\tau} e^-_\tau - (e^-_\tau)^* L^{-+}_{\tau,t} e^+_t \\ & - (e^-_t)^* L^{-+}_{t,\tau} e^+_\tau - (e^-_\tau)^* L^{--}_{\tau,t} e^-_t + (e^-_t)^* L^{--}_{t,\tau} e^-_\tau],\end{aligned} \tag{14}$$

where we have skipped the site indices for brevity. The above expression for the current response is formally exact; however, the averaging over the fields gives contributions in increasing powers of the tunneling conductance with the leading order corresponding to the atomic limit.

III. NONEQUILIBRIUM AC CURRENT RESPONSE

We are interested in the current response of our infinite array deep in the Mott-insulator regime $g \ll 1$ where transport is dominated by $O(g)$ sequential tunneling terms since at any order in tunneling, the cost $2E_C$ for creating a particle-hole pair is always paid. In contrast, higher-order tunneling effects are important in short arrays or where $g \gtrsim 1$. Interdot tunneling processes also lead to the renormalization of the charging energy E_C due to virtual tunneling to nearby dots. It is known that such processes result in $O(g)$ corrections to E_C, which for $g \ll 1$ do not make a qualitative difference to our findings except for replacing E_C by its renormalized value [39]. In contrast, when $g \sim O(1)$, the effect of the surrounding dots becomes important, and indeed, Coulomb blockade effects tend to get washed out, and the current response becomes resistive [36].

In the rest of our analysis, we will compute only the leading-order contribution to the current response. Figure 2 provides a pictorial illustration of why higher-order tunneling effects are not significant in infinite quantum dot arrays deep in the Mott-insulator regime.

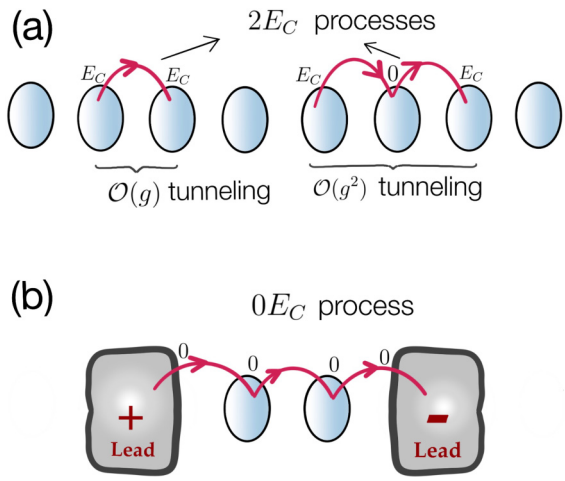

FIG. 2. (a) Illustration of the dominance of single-link tunneling processes in transport in the infinite chain deep in the Mott-insulating regime. Since a Coulomb blockade cost has to be always paid for creating a particle-hole pair at different sites, the single-link tunneling process that is $O(g)$ dominates higher-order processes. In (b), a system with a small number of dots is shown. Here a higher-order cotunneling process from source to drain leads allows one to circumvent the Coulomb blockade at the dots since only virtual excitations occur in the intermediate dots. Note that the leads by definition have zero charging energy.

Instead of working with the charging action of Eq. (6) that involves only the phases, it is convenient to work with a number-phase representation. For this, we rewrite the action in Eq. (6) as $\int_t [1/2E_C(\partial_t\phi_k^c)(\partial_t\phi_k^q) + N_0\partial_t\phi_k^q]$ and decouple the first term introducing the Hubbard-Stratonovich fields $n_k^{q,c}$,

$$S_C[n,\phi] = \sum_k \int_t \left([n_k^c + N_0]\partial_t\phi_k^q + n_k^q\partial_t\phi_k^c - 2E_C n_k^c n_k^q\right). \tag{15}$$

Here $n_k^{c(q)}$ is the classical (quantum) component of the charge excitation on the kth dot and is conjugate to $\phi_k^{q(c)}$. At this stage, the charge variable n is unconstrained. We allow for finite winding numbers in ϕ_k^q,

$$\phi_k^q(t) \to \frac{2\pi W_k}{T_0}(t - T_0) + \phi_k^q(t), \tag{16}$$

where T_0 is a timescale longer than any others in the problem and the phase on the right-hand side satisfies Dirichlet boundary conditions $\phi_k^q(0) = \phi_k^q(T_0) = 0$. Summing over the winding numbers forces n_k^c to take only integer values. An in-depth discussion of the charge quantization emerging from such considerations can be found in the literature, for example, in the textbook Ref. [38].

Performing the average with respect to the phase fields $\int D\phi\, \hat{j}_{k,1}[\phi]e^{iS}$ yields the expectation value $j(t)$ for the current. To leading order in the perturbation series, the averaging requires calculation of bare bond correlators defined as

$$\Pi^{(0)}_{\sigma\sigma'}(t,t') = \left\langle \exp\left[-i\phi^{\sigma}_{k,1}(t) + i\phi^{\sigma'}_{k,1}(t')\right]\right\rangle_0, \tag{17}$$

where $\langle\cdots\rangle_0$ denotes averaging with the bare action. The bare bond correlator can be factorized into a product of two single-site correlators,

$$\Pi^{(0)}_{\sigma\sigma'}(t,t') = C_{\sigma\sigma'}(t,t')C_{\sigma'\sigma}(t',t), \tag{18}$$

where

$$C_{\sigma\sigma'}(t,t') = \left\langle \exp\left[-i\phi^{\sigma}_{k}(t) + i\phi^{\sigma'}_{k}(t')\right]\right\rangle_0, \tag{19}$$

and the site correlators can be shown to be [6]

$$C_{\pm\pm}(t,t') = \exp[\mp iE_C|t-t'|], \tag{20}$$

$$C_{\pm\mp}(t,t') = \exp[\pm iE_C(t-t')]. \tag{21}$$

The expectation value of the current response so obtained is

$$j(\tau) = ig\int_{-\infty}^{\tau} e^{iA^c_{k,1}(\tau) - iA^c_{k,1}(t)}\left\{\Sigma^R_{(\tau-t)}\cos[2E_C(\tau-t)] - i\Sigma^K_{(\tau-t)}\sin[2E_C(\tau-t)]\right\}dt + \text{c.c.} \tag{22}$$

We use $A^c_{k,1}(t) = \frac{V}{\Omega}\cos(\Omega t)$ and expand the exponentials containing the vector potential making use of the Jacobi-Anger formula $e^{iz\cos(x)} = \sum_{n=-\infty}^{\infty} i^n J_n(z)e^{inx}$ and perform the time integrals to obtain our final expression for $j(\tau)$ following the quench,

$$\begin{aligned} j(t) = &-\frac{4gE_C}{\pi^2}\left(\sin\left(\frac{V}{\Omega}\cos(\Omega t)\right)\left\{\text{Ci}(2E_Ct)\left[1 - J_0\left(\frac{V}{\Omega}\right)\right] - \text{sinc}(2E_Ct)\right\} - \sin\left(\frac{V}{\Omega}[1-\cos(\Omega t)]\right)\text{sinc}(2E_Ct)\right) \\ &-\frac{4gE_C}{\pi^2}\sin\left(\frac{V}{\Omega}\cos(\Omega t)\right)J_0\left(\frac{V}{\Omega}\right)\ln\left(\frac{2E_C}{\Omega}\right) - \frac{2g\Omega}{\pi^2}\sum_{n=1}^{\infty}(-1)^n J_n\left(\frac{V}{\Omega}\right)\sin\left(\frac{V}{\Omega}\cos(\Omega t) + \frac{n\pi}{2}\right) \\ &\times\left[\left(\frac{2E_C}{\Omega} - n\right)I_n(t) + \left(\frac{2E_C}{\Omega} + n\right)I_{-n}(t) + \cos(n\Omega t)\left\{\left(\frac{2E_C}{\Omega} - n\right)\ln\left|\frac{2E_C}{\Omega} - n\right| + \left(\frac{2E_C}{\Omega} + n\right)\ln\left(\frac{2E_C}{\Omega} + n\right)\right\}\right]. \end{aligned} \tag{23}$$

Here the J_n are Bessel functions of the first kind, $\text{sinc}(y) = \sin y/y$, $I_n(t) = -\text{Ci}[(2E_C - n\Omega)t]\cos(n\Omega t) + \text{si}[(2E_C - n\Omega)t]\sin(n\Omega t)$, and the functions Ci and si, respectively, are the trigonometric integrals $\text{Ci}(y) = -\int_y^{\infty} dx\, \cos x/x$ and $\text{si}(y) = -\int_y^{\infty} dx\, \sin x/x$. We have used here the standard notation for the trigonometric integrals, the sine counterpart, $\text{Si}(y) = \int_0^y dx\, \sin(x)/x$, of $\text{Ci}(y)$ is related to $\text{si}(y)$ through $\text{Si}(y) = (\pi/2) + \text{si}(y)$.

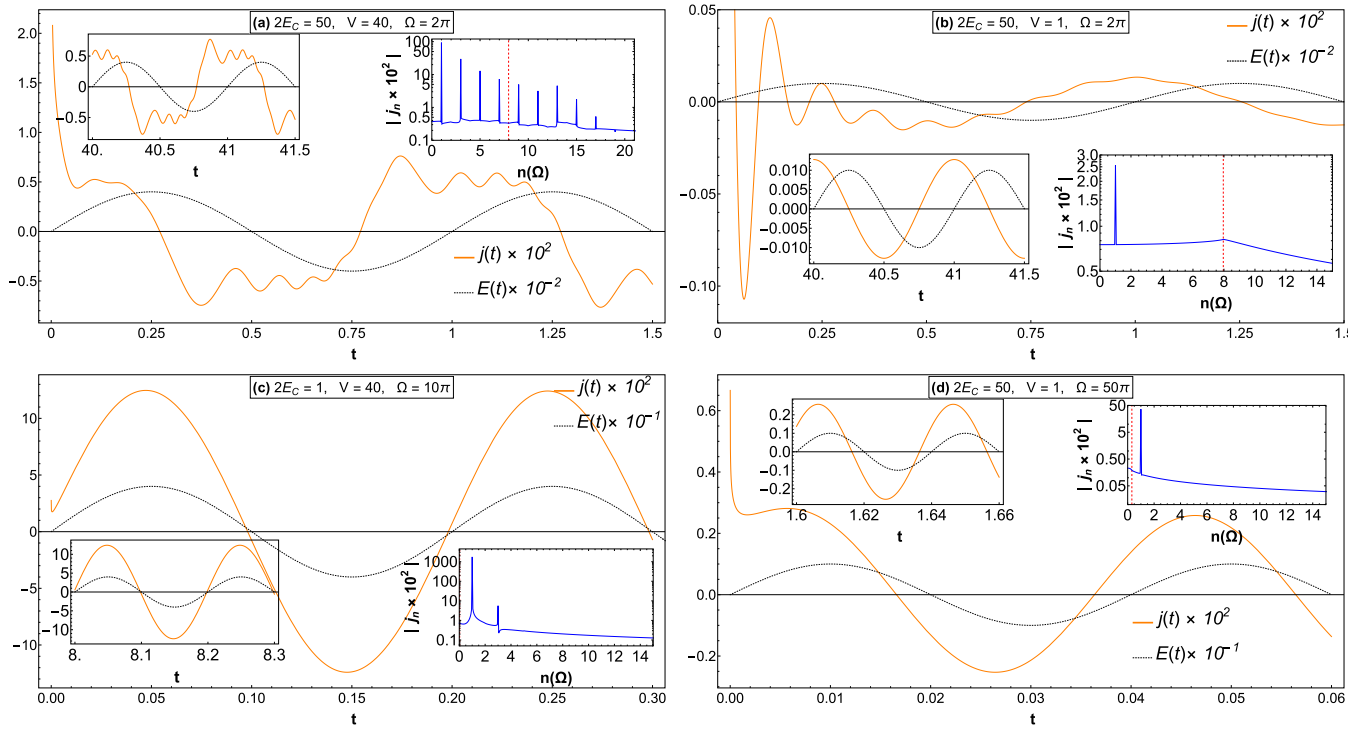

FIG. 3. Plots showing the transient current response j (solid curves) vs time t following an ac quench (dotted curves) in different regimes of the parameters $2E_C/\Omega$ and V/Ω. The left insets in (a)–(d) show the late time current response (solid curves) together with the ac field (dotted curves), and the right insets show the power spectrum of the current response as a function of frequency in units of the driving field frequency Ω. The dashed vertical lines in the power spectrum plots indicate the position of $2E_C$ corresponding to the Bloch-like oscillations [visible only in (b) where ac-induced charge fluctuations are weak]. Peaks at odd multiples of Ω are seen in the power spectra when $V/\Omega \gg 1$, and correspond to multiphoton-assisted tunneling processes. In (c), the long time current response is in phase with the drive, such as a resistor, whereas in the other cases, there is a finite phase difference.

The physical significance of the different contributions to the current in Eq. (23) may be understood as follows. The first line in Eq. (23) describes Bloch-like oscillations at a frequency $2E_C$. The amplitude of the Bloch-like oscillations, a signature of charge quantization, falls inversely with time following the quench owing to the presence of dissipation. Such decay of Bloch oscillations is not seen in KDMFT studies of dissipationless half-filled Hubbard chains [7] and could be a consequence of insufficiently long waiting time in the numerical simulations.

At long times, only the contributions from the last three lines of Eq. (23) survive and the NESS current is obtained by simply making the substitution,

$$(2E_C/\Omega - n)I_n(t) + (2E_C/\Omega + n)I_{-n}(t) \rightarrow -\pi(n - 2E_C/\Omega)\Theta(n - 2E_C/\Omega)\sin(n\Omega\tau).$$

The parameter $2E_C/\Omega$ is the number n of photons required to excite an electron through the Mott gap, whereas V/Ω controls the strength $J_n(V/\Omega)$ of an n-photon process. The logarithmic singularities at the thresholds $n\Omega = 2E_C$ are not the expected response of a gapped system but reflect the collective response of the dot electrons upon a tunneling event, similar to the x-ray edge phenomenon. The similarity with x-ray edge singularity is there because each dot has a large number of electrons and every tunneling event shifts the entire electron band by a large amount E_C.

Figure 3 shows the transient current response $j(t)$ following the ac quench in four different parameter regimes. The left insets in (a)–(d) show the late time current response together with the ac field, whereas the right insets show the power spectrum of $j(t)$ as a function of frequency, measured in units of Ω. The power spectra all show a peak at Ω, and for stronger field strengths $V/\Omega > 1$, higher harmonics appear at odd integer multiples of Ω corresponding to multiphoton processes. The vertical dashed lines in the power spectra indicate the position of $2E_C$ at which the Bloch-like oscillations, a signature of charge quantization, occur.

Figures 3(a) and 3(b) correspond to $2E_C/\Omega \gg 1$ where the Mott gap greatly exceeds the driving frequency. In both cases the phase of the current response is approximately $\pi/2$ ahead of the driving field, which, in combination with the insulating frequency dependence (see the analysis below), resembles a capacitor. The power spectrum of the current in Fig. 3(a), where $V/\Omega > 1$, shows significant multiphoton peaks, but a distinct signature of the Bloch-like oscillations at $2E_C$ is not evident. In contrast, the Bloch-like peak at $2E_C$ is clearly visible in Fig. 3(b) where $V/\Omega < 1$ so that multiphoton processes that could excite electrons across the Mott gap are suppressed. Since power dissipation is governed by the component of the current that is in phase with the driving field, both (a) and (b) correspond to weak dissipation. In Fig. 3(c), where $2E_C/\Omega \ll 1$ and $V/\Omega > 1$, charge excitations induced by both single and multiphoton processes are significant. The

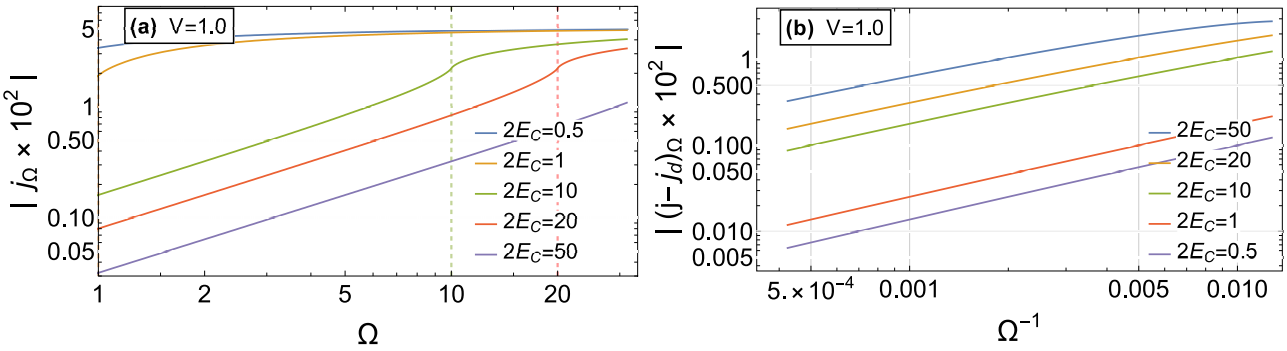

FIG. 4. Plots showing the frequency dependence of the single-photon component j_Ω of the current for a given ac electric-field $V = 1$. In (a), a capacitative Mott-insulator type response $|j_\Omega| \sim \Omega$ is seen at low frequencies ($2E_C/\Omega \gg 1$) and weak electric fields ($2E_C/V \gg 1$). Singularities in j_Ω appear at $\Omega = 2E_C$ separating insulator- and conductor-like behavior of the current. In (b), the behavior of j_Ω at high frequencies and low fields $2E_C/\Omega$, $V/\Omega \ll 1$ is like a resistively shunted inductor, i.e., $|(j - j_d)_\Omega| \sim \Omega^{-1}$, where j_d is the dissipative component of the current.

current response is predominantly at the driving frequency, and in phase with the ac field, much like a resistor, which one would expect [33] due to pair production facilitated by the small Mott gap and large electric-field strength. In Fig. 3(d), the large driving frequency implies single-photon-dominated charge excitations. We show below that the frequency dependence is that of a resistively shunted inductor. Similar odd harmonic generation and multiphoton-assisted tunneling phenomena have also been reported in recent KDMFT-based numerical studies [7,11,40].

We now examine the limits where the current response is capacitative or inductive. For simplicity we consider the single-photon-dominated regimes where $V/\Omega \ll 1$, and Eq. (23) for the NESS current simplifies to ($x = 2E_C/\Omega$),

$$j \approx V \frac{2g}{\pi^2} \begin{cases} \frac{1}{x}\cos(\Omega t), & x \gg 1, \\ \frac{\pi}{2}\sin(\Omega t) + x \ln\left(\frac{1}{x}\right)\cos(\Omega t), & x \ll 1. \end{cases} \quad (24)$$

At low frequencies where $x \gg 1$, the current is proportional to the derivative of the driving field—a capacitative response characteristic of a Mott insulator. At high frequencies, $x \ll 1$, single-photon processes are sufficient to ensure charge excitations across the Mott gap, and the current is approximately linear-response type, having components proportional to the driving field as well as to its time integral. Apart from an additional enhancement by a factor $\ln(\Omega/2E_C)$, it is essentially that of a resistively shunted inductor, with *negative* link inductance $L \sim -[gE_C \ln(\Omega/2E_C)]^{-1}$. Although this behavior also superficially resembles that of a classical *RC* series circuit; however, the $1/\Omega$ term there has a very different dependence on gE_C, which is the interdot Thouless energy of diffusion of a particle-hole pair. This parameter enters our expression in a manner similar to the Josephson energy in superconductor dot arrays. The inductive response is also unrelated to the surface-plasmon related Mie resonance that occurs in the same system [41]. As $x \to 0$, the current response is resistive and independent of E_C. Figure 4 shows the magnitude of the dominant single-photon component j_Ω of the current in both these frequency limits. Kinks in j_Ω curves are seen at $\Omega = 2E_C$. The logarithmic nonanalyticities separating insulating and metallic frequency dependence of the linear-response current indicate an insulator to metal transition.

Figure 5 shows the behavior of the frequency derivative $\partial|j_\Omega|/\partial\Omega$ of the single-photon component of the current response as a function of the distance from the threshold $\Omega = 2E_C$. This provides a clearer illustration of the frequency-driven insulator to metal transition. Upon crossing the threshold $\Omega = 2E_C$, the current response changes from insulating (capacitative) to metallic, which is seen in the increase and subsequent decrease in $\partial|j_\Omega|/\partial\Omega$ through the threshold. It is evident from the expression for the current response, Eq. (23) that the singularity in the current response at $\Omega = 2E_C$ is essentially logarithmic. The collapse of the curves for different parameter values indicates a universal singular response that depends only on the dimensionless frequency $\Omega/2E_C$.

Multiphoton processes become important at low frequencies $V/\Omega \gg 1$. This is evident in Fig. 3(a). We found that these processes are typically much smaller than the single-photon contribution. In Fig. 6 we present plots for the third harmonic (and the derivative) of the current response. The weak

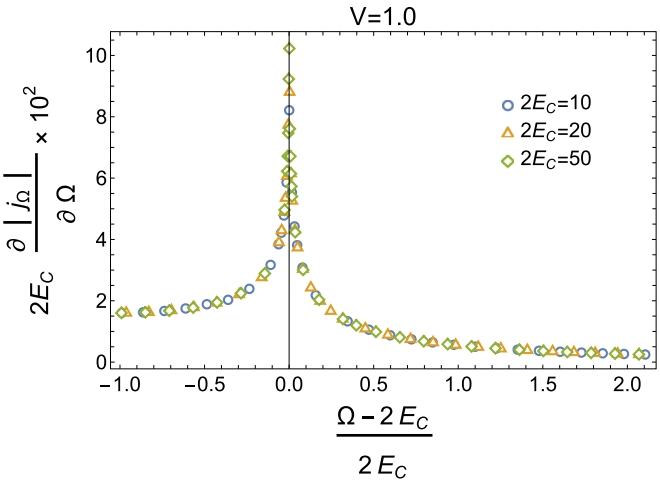

FIG. 5. Plot illustrating the behavior of $\partial|j_\Omega|/\partial\Omega$ in the presence of a purely ac drive for different values of E_C and a fixed value of $V = 1$. By rescaling the axes, the curves are seen to collapse, indicating a universal response that depends only on the dimensionless frequency $\Omega/2E_C$. The analytic dependence is given by Eq. (23).

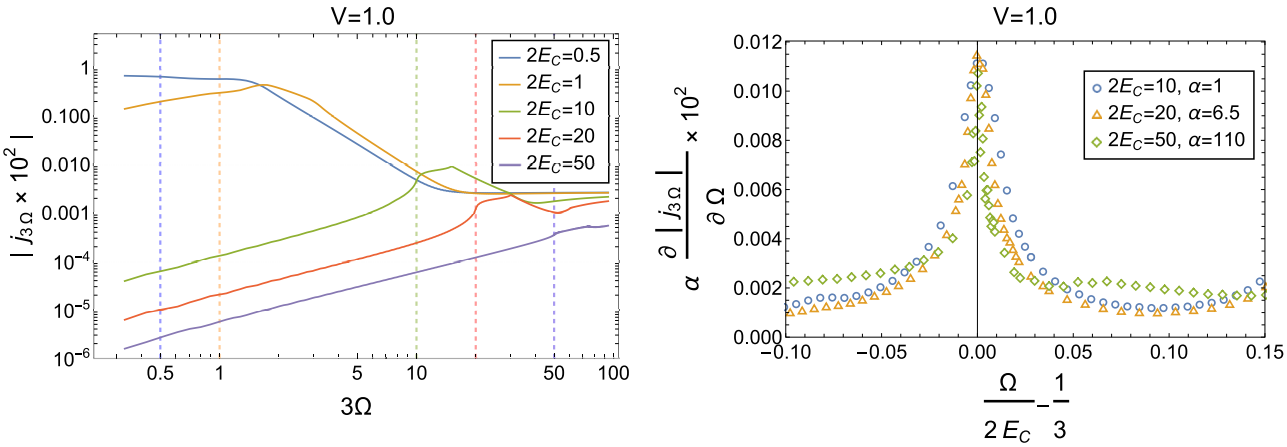

FIG. 6. The plot on the left shows the current response $j_{3\Omega}$ corresponding to the third harmonic, to be viewed in comparison with the linear-response component j_Ω. Kink-like features are seen when the threshold condition $3\Omega = 2E_C$ for three-photon excitation across the Mott gap is satisfied. Note that $j_{3\Omega}$ is much smaller than the linear-response component. The right plot shows the derivative of $j_{3\Omega}$ in the vicinity of the threshold. The singularity in the derivative of the current response is on account of the logarithmic singularities in the current response. The data collapse shows universality in the current response for different values of the Coulomb energy.

logarithmic singularities are present at the threshold $3\Omega = 2E_C$, and there is a scaling collapse at the threshold, similar to the single-photon case. The three-photon contribution is smaller than the dominant single-photon contribution by a factor of around 100.

This NESS response exhibits remarkable similarities with resistively shunted Josephson arrays. The high-frequency regime resembles that of a superconducting Josephson array albeit with *negative* stiffness $K = -gE_C \ln(\Omega/2E_C)$, amounting to π-phase slips in the links, such as an η-pairing phase [23]. This should be compared to the Ambegaokar-Baratoff relation $K = +g\Delta$ for the stiffness of the Josephson junction, where Δ is the gap to quasiparticle excitations in the dots. This effect is reminiscent of the reported ac-induced attractive electron interactions enhancement reported in studies of the optically excited half-filled Hubbard models [13–16,18–22]. Various groups have, subsequently, also reported the formation of an η-pairing state in the presence of significant doublon excitations [15,24,25]. Note, however, that in our case, although the resemblance with η pairing is there, it cannot be attributed to doublon production and condensation since the equilibrium electron number in the quantum dots is arbitrary. The question of existence of supercurrent can be addressed by looking for Shapiro steps in the current response under simultaneous ac and dc bias.

IV. NESS FOR SIMULTANEOUS AC AND DC BIAS

To probe whether there is indeed an ac-induced superconducting η-pairing state in our case, we analyze below the current response in the presence of a simultaneous dc field of strength D for which we choose

$$A^c_{k,1}(t) = \frac{V}{\Omega}\cos(\Omega t) + Dt. \tag{25}$$

The NESS current response for this case may be obtained following the same procedure outlined above for the ac response. The expression for $j(t)$, although straightforward to obtain, is rather cumbersome, and we introduce the following additional quantities to simplify its presentation:

$$\begin{aligned}
p_1 &= \pi\Theta(n\Omega - 2E_C - D)(n\Omega - 2E_C - D),\\
p_2 &= \pi\Theta(-n\Omega - 2E_C - D)(-n\Omega - 2E_C - D),\\
p_3 &= \pi\Theta(n\Omega - 2E_C + D)(n\Omega - 2E_C + D),\\
p_4 &= \pi\Theta(-n\Omega - 2E_C + D)(-n\Omega - 2E_C + D),
\end{aligned}$$

and

$$\begin{aligned}
q_1 &= (n\Omega - 2E_C - D)\ln|n\Omega - 2E_C - D|,\\
q_2 &= (-n\Omega - 2E_C - D)\ln|-n\Omega - 2E_C - D|,\\
q_3 &= (n\Omega - 2E_C + D)\ln|n\Omega - 2E_C + D|,\\
q_4 &= (-n\Omega - 2E_C + D)\ln|-n\Omega - 2E_C + D|,
\end{aligned}$$

and $\theta_\pm = \frac{V}{\Omega}\cos(\Omega t) \pm n\Omega t$.

Now, introducing the quantities f_n and g_n,

$$\begin{aligned}
f_n &= p_1\cos\theta_+ + p_2\cos\theta_- - p_3\cos\theta_- - p_4\cos\theta_+\\
&\quad -q_1\sin\theta_+ - q_2\sin\theta_- - q_3\sin\theta_- - q_4\sin\theta_+,\\
g_n &= -p_1\sin\theta_+ - p_2\sin\theta_- + p_3\sin\theta_- + p_4\sin\theta_+\\
&\quad -q_1\cos\theta_+ - q_2\cos\theta_- - q_3\cos\theta_- - q_4\cos\theta_+,
\end{aligned}$$

we present our final expression for the current response in the presence of a simultaneous dc and ac bias,

$$j(t) = \frac{g}{2\pi^2}J_0\left(\frac{V}{\Omega}\right)f_0 - \frac{g}{\pi^2}\sum_{n=4k,\,k=0}^{k=\infty}\left\{J_n\left(\frac{V}{\Omega}\right)f_n - J_{n+1}\left(\frac{V}{\Omega}\right)g_{n+1} - J_{n+2}\left(\frac{V}{\Omega}\right)f_{n+2} + J_{n+3}\left(\frac{V}{\Omega}\right)g_{n+3}\right\}. \tag{26}$$

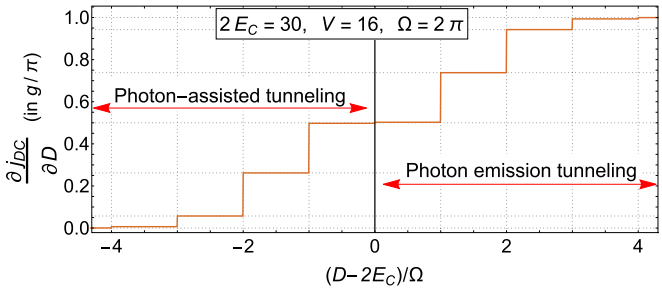

FIG. 7. Plot showing photon-assisted tunneling and stimulated photon emission phenomena in the presence of a simultaneous ac drive $V\sin(\Omega t)$ and dc bias $D > 0$. The y axis shows the leading contribution to dc transconductance $\partial j_{\rm dc}/\partial D$ as a function of the dc bias. For $D < 2E_C$, the steps correspond to tunneling assisted by absorption of one or more photons, and for $D > 2E_C$, to tunneling with stimulated photon emission. The threshold for the finite dc current is at $D/\Omega = [2E_C/\Omega] + 1$. At large dc bias, the dc conductance approaches g/π signifying strong charge fluctuations and the absence of Coulomb blockade. Comparing with driven Josephson junctions, E_C plays the role of the single-particle gap Δ.

Here, $J_n(x)$ are Bessel's function of the first kind. To get the dc component $j_{\rm dc}$ we numerically average the current over a large time interval. The dc transconductance is $\frac{\partial j_{\rm dc}}{\partial D}$.

We observe jumps in the dc transconductance $\frac{\partial j_{\rm dc}}{\partial D}$ at specific values of the dc potential difference across a link $D = D_n$,

$$|D_n| - 2E_C = n\Omega, \tag{27}$$

where n is an integer, such as the photon-mediated tunneling steps in the IV characteristics of resistively shunted Josephson arrays [28]. The role of the quasiparticle gap Δ in the Josephson case is taken by the Coulomb scale E_C here. However, in contrast with the Josephson case, additional Shapiro steps that appear in intervals of $\Omega/2$ and are associated with the supercurrent, are absent here. For $n > 0$, dc transport occurs through stimulated emission of photons whereas for $n < 0$, photon-assisted tunneling takes place. Figure 7 shows the dc transconductance when a simultaneous dc bias D is also applied. In the absence of the ac field, the dc transconductance is known to have a threshold behavior [27], vanishing for $|D| < 2E_C$ and assuming the value of g/π for $|D| > 2E_C$. When the ac drive is also turned on, the threshold shifts to a lower value, and transconductance is zero for $|D|/\Omega < [2E_C/\Omega] + 1$, where $[a]$ is the greatest integer less than or equal to a. This process is photon-assisted tunneling. When $|D| > 2E_C$, steps continue to appear in the transconductance but now they are associated with tunneling accompanied by stimulated photon emission.

V. DISCUSSION

To summarize, we showed that the current response to an ac drive in our dissipative Mott-insulator chain undergoes a transition from an insulator frequency dependence at low frequencies $\Omega/2E_C \ll 1$ to a conducting diamagnetic frequency dependence for high-frequencies $\Omega/2E_C \gg 1$ with an effective phase stiffness $K \sim gE_C$, the Thouless energy for interdot diffusion of a particle-hole pair. The transition occurs at the threshold $\Omega = 2E_C$ for photon-assisted transition across the Mott gap. The presence of a large number of electrons in the dots results in characteristic logarithmic singularities reminiscent of x-ray edge phenomena in atomic physics. At high frequencies the sign of the diamagnetic response is negative and resembles η pairing [23] in the half-filled Hubbard chain. We argued that the η-pairing-like behavior in our model is not due to superconductivity but a consequence of strong charge fluctuations brought about by the nonequilibrium drive. This view is confirmed by the absence of Shapiro steps, a key signature of supercurrent, and the fact that despite the diamagnetic behavior at high frequencies, the charge stiffness is zero.

For our analysis, we employ an analytical Keldysh field-theory approach based on the Ambegaokar-Eckern-Schön rotor model for studying electronic transport in quantum dot arrays. Our technique correctly reproduces a number of known results on optically driven Hubbard chains (e.g., Bloch-like oscillations, odd harmonic generation, and apparently attractive Coulomb correlations) obtained in numerical Keldysh-DMFT studies of optically excited half-filled Hubbard chains. However, in contrast with the numerical studies, we find a slow power-law decay of the Bloch-like oscillations. This could have been missed in earlier DMFT studies due to insufficient time lapse in the simulations following a quench.

Our treatment suggests that caution must be exercised in using optical properties to determine the existence of η pairing in driven Hubbard chains. An alternate physical explanation that emerges from our paper is that most of the reported superconductor-like optical properties do not, in fact, require the existence of superconducting order but rather are a consequence of number-phase duality effects that are common between Mott insulators and superconductors. To establish the existence of superconductivity, additional evidence, such as the existence of the supercurrent (through Shapiro steps or otherwise) or other direct evidence of off-diagonal long-range order is required.

ACKNOWLEDGMENTS

We thank S. Sankar for his valuable comments.

APPENDIX: DERIVATION OF THE PHASE MODEL

Here we sketch the steps leading from the microscopic Hamiltonian of Eq. (1) to the phase model. We first perform the Hubbard-Stratonovich decoupling of the Coulomb interaction,

$$\exp\left(-i\int_t H_C\right) = \exp\left[-i\sum_k \int_t E_C\left(\sum_\alpha c^\dagger_{k,\alpha}c_{k,\alpha} - N_0\right)\left(\sum_\alpha c^\dagger_{k,\alpha}c_{k,\alpha} - N_0\right)\right]$$
$$\propto \int DV_k \exp\left\{i\sum_k \int_t \frac{1}{4E_C}\left[V_k - 2E_C\left(\sum_\alpha c^\dagger_{k,\alpha}c_{k,\alpha} - N_0\right)\right]^2\right\}\exp\left(-i\int_t H_C\right). \tag{A1}$$

Since we are interested in the nonequilibrium response, we go over to the Keldysh action formalism and label the fields on the forward and backward time contours, respectively, by superscripts + and −. The Hubbard-Stratonovich fields cause large shifting of the entire electron energy bands during tunneling events. To eliminate these fields we perform gauge transformations $c^\pm_k \to e^{-i\phi^\pm_k}c^\pm_k$ on the fermion fields such that $\partial_t\phi^\pm_k = V^\pm_k$. Although the Hubbard-Stratonovich fields get eliminated from the single-electron energies, they clearly appear now in the interdot tunneling terms. It is convenient to perform here a basis rotation in Keldysh space so that the Green's functions (see below) have the customary retarded, advanced, or Keldysh forms. To this end we introduce the classical (c) and quantum (q) components,

$$V^c = \tfrac{1}{2}(V^+ + V^-), \quad V^q = V^+ - V^-, \tag{A2}$$

$$c^c = \tfrac{1}{\sqrt{2}}(c^+ + c^-), \quad c^q = \tfrac{1}{\sqrt{2}}(c^+ - c^-), \tag{A3}$$

$$(c^c)^\dagger = \tfrac{1}{\sqrt{2}}[(c^+)^\dagger - (c^-)^\dagger], \quad (c^q)^\dagger = \tfrac{1}{\sqrt{2}}[(c^+)^\dagger + (c^-)^\dagger], \tag{A4}$$

$$\Psi = \begin{pmatrix} c^c \\ c^q \end{pmatrix}, \quad \Psi^\dagger = \begin{pmatrix} (c^c)^\dagger & (c^q)^\dagger \end{pmatrix}. \tag{A5}$$

The Keldysh action $S = S_0 + S_C + S_{\rm tun}$ now takes the form

$$S_0 = \sum_{k,\alpha}\int_t \Psi^\dagger_{k,\alpha}\begin{bmatrix} i\partial_t + i\eta + \mu - \epsilon_\alpha & 2i\eta F_k \\ 0 & i\partial_t - i\eta + \mu - \epsilon_\alpha \end{bmatrix}\Psi_{k,\alpha}, \tag{A6}$$

$$S_C = \sum_k \int_t \left(\frac{1}{2E_c}\partial_t\phi^c_k\partial_t\phi^q_k + N_0\partial_t\phi^q_k\right), \tag{A7}$$

$$S_{\rm tun} = \sum_{k,\alpha,\beta}\int_t \left[t^{\alpha,\beta}_{k,k+1}\bar\Psi_{k\alpha}\exp(-i\hat\phi_{k,1})\Psi_{k+1,\beta} + \text{c.c.}\right], \tag{A8}$$

where $\hat\phi_{k,1} = \hat\phi_{k+1} - \hat\phi_k$ with $\hat\phi_k = \phi^c_k + (1/2)\phi^q_k\sigma_1$. Here, $F_k(t,t')$ is related to the noninteracting distribution function of electrons in the kth dot. If the number of dot electrons is large, then it can be shown [6] that F_k can be approximated by its equilibrium value $F_k(t-t')$. In the frequency domain, this function is given by $F(\omega) = 1 - 2f(\omega)$, where $f(\omega)$ is the Fermi-Dirac distribution function. The infinitesimally small positive constant η has been added for the theory to have proper causal structure.

The fermion-bilinear part of the action $S_F = S_0 + S_{\rm tun}$ can be integrated out easily. Let fermion Lagrangian density be $L_F = \Psi^\dagger\hat G^{-1}\Psi$ with

$$\hat G^{-1} = \hat G_0^{-1} + \hat T, \tag{A9}$$

where

$$(\hat G_0)^{-1}_{k,\alpha;k,\alpha} = \begin{pmatrix} \left(g^R_{k,\alpha}\right)^{-1} & 2\imath\eta F_k \\ 0 & \left(g^A_{k,\alpha}\right)^{-1} \end{pmatrix}, \tag{A10}$$

$$\hat T_{k,\alpha;k+1,\beta} = t^{\alpha\beta}_{k,k+1}e^{-i\hat\Phi_{k,1}}. \tag{A11}$$

The diagonal elements are the inverse retarded and advanced Green's functions,

$$\left(g^{R,A}_{k,\alpha}\right)^{-1} = i\partial_t \pm i\eta + \mu - \epsilon_\alpha, \tag{A12}$$

respectively. The interdot hopping matrix $\hat T$ is diagonal in Keldysh space as well as in the time indices. We integrate out the fermions and get $Z = \int D\phi\ \exp\{iS_C[\phi] + \text{tr}\ \ln(i\hat G^{-1})\}$ where we express the fermionic determinant as

$$\ln(\hat G^{-1}) = \ln(1 + \hat G_0\hat T) + \ln\left(\hat G_0^{-1}\right). \tag{A13}$$

Now, to obtain the action in terms of the phase fields, we perform a Taylor expansion of $\ln(1+\hat{G}_0\hat{T})$ in increasing powers of the tunneling. The first term clearly vanishes as $\hat{G}_0$ is diagonal in k and $T_{k;k}=0$. Up to second order in $\hat{T}$, we have

$$Z=\int D\phi\ \exp(iS_C[\phi]+iS_{\rm tun}[\phi]),\quad S_{\rm tun}[\phi]=\frac{i}{2}{\rm tr}(\hat{G}_0\hat{T}\hat{G}_0\hat{T}). \tag{A14}$$

Here $\hat{G}_0$ has the following structure in the Keldysh space:

$$(\hat{G}_0)_{k,\alpha;k,\alpha}(t,t')=\begin{pmatrix} g^R_{k,\alpha} & F_k\big(g^R_{k,\alpha}-g^A_{k,\alpha}\big)\\ 0 & g^A_{k,\alpha}\end{pmatrix}(t,t'), \tag{A15}$$

where

$$g^{R,A}_{k,\alpha}(t,t')=\frac{1}{2\pi}\int_\omega g^{R,A}_{k,\alpha}(\omega)e^{-i\omega(t-t')}=\int_\omega\frac{e^{-i\omega(t-t')}}{\omega\pm i\eta+\mu-\epsilon_\alpha}. \tag{A16}$$

We assume the matrix elements of $\hat{T}$ are independent of the energy indices, and, furthermore, we replace the discrete summation over the energy indices by integrals thereby obtaining expression for ${\rm tr}(\hat{G}_0\hat{T}\hat{G}_0\hat{T})$ in terms of $G^{R,A}(\omega)=\frac{1}{2\pi}\int_\epsilon g^{R,A}_{k,\epsilon}(\omega)$. In replacing the discrete sum over energies by an integral over a continuum, the time scales of interest should not exceed the inverse of the mean level spacing, or the Ehrenfest time. For longer time scales, quantum interference effects would become relevant even for ballistic, chaotic dots (see Ref. [42]). Denoting the mean-square tunneling matrix connecting pairs of levels in the neighboring sites as $|t|^2$, we obtain $S_{\rm tun}\propto g=\pi^2|t|^2/\delta^2$ and given by

$$S_{\rm tun}[\phi]=g\sum_k\int_{t,t'}\begin{pmatrix}e^{-i\phi^+_{k,1}} & e^{-i\phi^-_{k,1}}\end{pmatrix}_t L_{k,1}(t-t')\begin{pmatrix}e^{i\phi^+_{k,1}}\\ e^{i\phi^-_{k,1}}\end{pmatrix}_{t'}, \tag{A17}$$

where

$$L=\frac{1}{4}\begin{pmatrix}\Sigma^R+\Sigma^A+\Sigma^K & \Sigma^R-\Sigma^A-\Sigma^K\\ -\Sigma^R+\Sigma^A-\Sigma^K & -\Sigma^R-\Sigma^A+\Sigma^K\end{pmatrix}. \tag{A18}$$

The functions $\Sigma^{R,A}$ have a causal structure, such as the $G^{R,A}$ and are given by

$$\Sigma^{R(A)}_{k,1}(t)=i\big[G^{R(A)}(t)G^K_k(-t)+G^K_{k+1}(t)G^{A(R)}(-t)\big], \tag{A19}$$

$$\Sigma^K_{k,1}(t)=i\big[G^K_k(-t)G^K_{k+1}(t)-(G^R-G^A)_t(G^R-G^A)_{-t}\big], \tag{A20}$$

where the Keldysh component $G^K_k=F_k(G^R-G^A)$. Note that the kernel L involves products of single-fermion Green's functions and, thus, represents a bosonic propagator. It takes a very simple form in the frequency domain.

We make use of the following identities in the frequency domain to simplify the L matrix elements:

$$(G^R-G^A)_\epsilon=-i, \tag{A21}$$

$$\int_\epsilon\frac{1}{2\pi}[F(\epsilon+\omega)-F(\epsilon)]=\frac{\omega}{\pi}, \tag{A22}$$

$$\int_\epsilon\frac{1}{2\pi}[1-F(\epsilon-\omega)F(\epsilon)]=\frac{\omega}{\pi}F_b(\omega), \tag{A23}$$

where $F_b(\omega)=1+2f_b(\omega)$ and $f_b(\omega)$ is the equilibrium Bose-Einstein distribution function. Above identities enables us to make a simplification as follows:

$$\big(\Sigma^R_{k,1}-\Sigma^A_{k,1}\big)_\omega=\frac{i}{\pi}\omega, \tag{A24}$$

$$\big(\Sigma^K_{k,1}\big)_\omega=\frac{i}{\pi}\omega F_b(\omega). \tag{A25}$$

We now justify dropping the higher-order tunneling terms, such as ${\rm tr}(\hat{G}_0\hat{T}\hat{G}_0\hat{T}\hat{G}_0\hat{T}\hat{G}_0\hat{T})$ in the large-$\mathcal{N}$ approximation. Physically, the tunneling matrix elements $t^{\alpha\beta}_{kk'}$ must scale as $1/\mathcal{N}$ (where $\mathcal{N}$ is on the order of the number of conduction electrons in a dot) so that the dimensionless interdot conductance $g\sim|t|^2/\delta^2$ is independent of $\mathcal{N}$ and physically meaningful. Higher-order terms do not contribute in the large-$\mathcal{N}$ limit. For example, in the aforementioned fourth-order term, the tunneling elements contribute an overall scaling factor of $1/\mathcal{N}^4$ whereas the sum over internal indices contributes only a scaling factor of $\mathcal{N}^3$, resulting in this term becoming insignificant in the large-$\mathcal{N}$ sense. For a detailed analysis of the role of large $\mathcal{N}$, we refer to the arguments given in Ref. [6].

[1] S. Sayyad, R. Žitko, H. U. R. Strand, P. Werner, and D. Golež, Phys. Rev. B **99**, 045118 (2019).

[2] Y. Nomura, S. Sakai, M. Capone, and R. Arita, Sci. Adv. **1**, e1500568 (2015).

[3] M. Eckstein and P. Werner, Phys. Rev. Lett. **110**, 126401 (2013).
[4] S. Wall, D. Brida, S. R. Clark, H. P. Ehrke, D. Jaksch, A. Ardavan, S. Bonora, H. Uemura, Y. Takahashi, T. Hasegawa *et al.*, Nat. Phys. **7**, 114 (2011).
[5] N. Tsuji, T. Oka, and H. Aoki, Phys. Rev. B **78**, 235124 (2008).
[6] S. Sankar and V. Tripathi, Phys. Rev. B **99**, 245113 (2019).
[7] Y. Murakami and P. Werner, Phys. Rev. B **98**, 075102 (2018).
[8] A. V. Joura, J. K. Freericks, and A. I. Lichtenstein, Phys. Rev. B **91**, 245153 (2015).
[9] W.-R. Lee and K. Park, Phys. Rev. B **89**, 205126 (2014).
[10] M. Eckstein and P. Werner, J. Phys.: Conf. Ser. **427**, 012005 (2013).
[11] M. Eckstein, T. Oka, and P. Werner, Phys. Rev. Lett. **105**, 146404 (2010).
[12] C. Sow, S. Yonezawa, S. Kitamura, T. Oka, K. Kuroki, F. Nakamura, and Y. Maeno, Science **358**, 1084 (2017).
[13] F. Peronaci, O. Parcollet, and M. Schiró, Phys. Rev. B **101**, 161101(R) (2020).
[14] J. Li, D. Golez, P. Werner, and M. Eckstein, Phys. Rev. B **102**, 165136 (2020).
[15] T. Kaneko, T. Shirakawa, S. Sorella, and S. Yunoki, Phys. Rev. Lett. **122**, 077002 (2019).
[16] P. Werner, J. Li, D. Golez, and M. Eckstein, Phys. Rev. B **100**, 155130 (2019).
[17] R. Fujiuchi, T. Kaneko, Y. Ohta, and S. Yunoki, Phys. Rev. B **100**, 045121 (2019).
[18] F. Görg, M. Messer, K. Sandholzer, G. Jotzu, R. Desbuquois, and T. Esslinger, Nature (London) **553**, 481 (2018).
[19] J. R. Coulthard, S. R. Clark, S. Al-Assam, A. Cavalleri, and D. Jaksch, Phys. Rev. B **96**, 085104 (2017).
[20] K. Ido, T. Ohgoe, and M. Imada, Sci. Adv. **3**, e1700718 (2017).
[21] N. Tsuji, T. Oka, P. Werner, and H. Aoki, Phys. Rev. Lett. **106**, 236401 (2011).
[22] A. Rosch, D. Rasch, B. Binz, and M. Vojta, Phys. Rev. Lett. **101**, 265301 (2008).
[23] C. N. Yang, Phys. Rev. Lett. **63**, 2144 (1989).
[24] T. Kaneko, S. Yunoki, and A. J. Millis, Phys. Rev. Research **2**, 032027 (2020).
[25] J. Tindall, B. Buča, J. R. Coulthard, and D. Jaksch, Phys. Rev. Lett. **123**, 030603 (2019).
[26] M. Lankhorst and N. Poccia, J. Supercond. Novel Magn. **29**, 623 (2016).
[27] T. Matsuura, K. Inagaki, and S. Tanda, J. Phys.: Conf. Ser. **129**, 012024 (2008).
[28] M. Tinkham, *Introduction to Superconductivity* (Courier, New York, 2004).
[29] Y. Murakami, M. Eckstein, and P. Werner, J. Phys. Soc. Jpn. **30**, 011183 (2020).
[30] F. Peronaci, M. Schiró, and O. Parcollet, Phys. Rev. Lett. **120**, 197601 (2018).
[31] T. Qin and W. Hofstetter, Phys. Rev. B **97**, 125115 (2018).
[32] P. Schmidt and H. Monien, arXiv:cond-mat/0202046.
[33] T. Oka, Phys. Rev. B **86**, 075148 (2012).
[34] V. Tripathi, A. Galda, H. Barman, and V. M. Vinokur, Phys. Rev. B **94**, 041104(R) (2016).
[35] T. Fukui and N. Kawakami, Phys. Rev. B **58**, 16051 (1998).
[36] I. S. Beloborodov, A. V. Lopatin, V. M. Vinokur, and K. B. Efetov, Rev. Mod. Phys. **79**, 469 (2007).
[37] V. Ambegaokar, U. Eckern, and G. Schön, Phys. Rev. Lett. **48**, 1745 (1982).
[38] A. Altland and B. D. Simons, *Condensed Matter Field Theory* (Cambridge University Press, Cambridge, UK, 2010).
[39] G. Falci, G. Schön, and G. T. Zimanyi, Phys. Rev. Lett. **74**, 3257 (1995).
[40] Y. Murakami, M. Eckstein, and P. Werner, Phys. Rev. Lett. **121**, 057405 (2018).
[41] V. Tripathi and Y. L. Loh, Phys. Rev. B **73**, 195113 (2006)
[42] V. Tripathi and D. E. Khmelnitskii, Phys. Rev. B **58**, 1122 (1998).